Identification of recombination losses and charge collection efficiency in a perovskite solar cell by comparing impedance response to a drift-diffusion model – Electronic Supplementary Information

Antonio Riquelme[a,#], Laurence J. Bennett[b,#], Nicola E. Courtier[b], Matthew J. Wolf[c], Lidia Contreras-Bernal[a], Alison B. Walker[c,*], Giles Richardson[b,*], Juan A. Anta[a,*]

[a] Área de Química Física, Universidad Pablo de Olavide, E-41013, Seville, Spain.

[b] Mathematical Sciences, University of Southampton, SO17 1BJ, UK.

[c] Department of Physics, University of Bath, BA2 7AY, UK

#Both authors contributed equally to this work

Experimental details

Perovskite solar devices with regular configuration (TiO_2/$MAPbI_3$/Spiro-OMeTAD)[1,2] were fabricated on FTO-coated glass (Pilkington–TEC15) patterned by laser etching. Before the deposition, the substrates were cleaned using Hellmanex® solution and rinsed with deionized water and ethanol. Thereupon, they were ultrasonicated in 2-propanol and dried by using compressed air. The TiO_2 blocking layer was deposited onto the substrates by spray pyrolysis at 450 °C, using a titanium diisopropoxide bis(acetylacetonate) solution (75% in 2-propanol, Sigma Aldrich) diluted in ethanol (1:14, v/v), with oxygen as carrier gas. The TiO_2 compact layer was then kept at 450 °C for 30 min for the formation of anatase phase. Once the samples achieve room temperature, a TiO_2 mesoporous layer was deposited by spin coating at 2000 rpm during 10 s using a commercial TiO_2 paste (Dyesol, 18NR-T) diluted in ethanol (1:5, weight ratio). After drying at 100 °C for 10 min, the TiO2 mesoporous layer was heated at 500 °C for 30 min and later cooled to room temperature. An additional doping

treatment using Li^+ ions (10.04 mg LiTFSI in 1 ml acetonitrile, 35mM) was used for the TiO2 mesoporous layer prior to $CsPbBr_3$ deposition.

For $MAPbI_3$ based devices, a pure methylammonium lead iodide solution were prepared to be deposited by spin coating using a methodology previously reported:[2] The perovskite precursor solution was adjusted to the relative humidity of the environment (42% R.H.) by the Pb/DMSO ratio. The perovskite precursor solution (50 μL) was spin-coated in a one-step setup at 4000 rpm for 50 s. During this step, DMF is selectively washed with non-polar diethyl ether just before the white solid begins to crystallize in the substrate. Spiro-OMeTAD was deposited as hole selective material by dissolving 72.3 mg in 1 mL of chlorobenzene as well as 17.5 μL of a lithium bis (trifluoromethylsulphonyl)imide (LiTFSI) stock solution (520 mg of LiTFSI in 1mL of acetonitrile), and 28.8 μL of 4-tert-butylpyridine (TBP). The Spiro-OMeTAD was spin coated at 4000 rpm for 30 s. The solution was filtered with a 0.2 μm PTFE filter prior to their deposition. Finally, 60 nm of gold was deposited as a metallic contact by thermal evaporation under a vacuum level between $1{\cdot}10^{-6}$ and $1{\cdot}10^{-5}$ torr. All the deposition processes were carried out outside a glovebox under environmental conditions.

Numerical Model

The simulated device consists of an electron transport layer, perovskite absorber layer and hole transport layer: ETL/$MAPbI_3$/HTL.[3] Within the perovskite layer ($0 < x < b$), the electron and hole densities, n and p respectively, are governed in time, t, and one spatial dimension, x, via the continuity equations

$$\frac{\partial n}{\partial t} - \frac{1}{q}\frac{\partial j_n}{\partial x} = G - R, \qquad j_n = qD_n\left(\frac{\partial n}{\partial x} - \frac{n}{k_B T}\frac{\partial \phi}{\partial x}\right), \tag{1}$$

$$\frac{\partial p}{\partial t} + \frac{1}{q}\frac{\partial j_p}{\partial x} = G - R, \qquad j_p = -qD_p\left(\frac{\partial p}{\partial x} + \frac{p}{k_B T}\frac{\partial \phi}{\partial x}\right), \tag{2}$$

where q is the elementary charge, G and R the generation and recombination rates respectively, $D_{n,p}$ the respective diffusion coefficients, k_B the Boltzmann constant and T is the temperature. The migration of the mobile anion vacancy density, P, within the perovskite layer is modelled by

$$\frac{\partial P}{\partial t} + \frac{\partial F_P}{\partial x} = 0, \qquad F_P = -D_P\left(\frac{\partial P}{\partial x} + \frac{P}{k_B T}\frac{\partial \phi}{\partial x}\right), \tag{3}$$

where F_P is the ionic flux and D_P is the anion vacancy diffusion coefficient. Equations (1-3) couple to Poisson's equation for the electric potential

$$\frac{\partial^2\phi}{\partial x^2} = \frac{q}{\epsilon_p}(N_0 - P + n - p). \quad (4)$$

Here, ϵ_p is the permittivity of the perovskite and N_0 is the uniform cation vacancy density which is equal to the mean anion vacancy density to ensure charge neutrality. Electrons and holes are generated within the perovskite via the Beer-Lambert profile for a single wavelength of light

$$G(x) = F_{ph}\alpha e^{-\alpha x}, \quad (5)$$

where F_{ph} is the flux of photons incident on the device with energy above the bandgap and α is the absorption coefficient of the perovskite. Recombination within the bulk of the perovskite is calculated using a combination of bimolecular (direct relaxation across the bandgap) and trap-assisted Shockley-Read-Hall (SRH) schemes, given by

$$R(n,p) = \beta(np - n_i^2) + \frac{(np - n_i^2)}{\tau_n p + \tau_p n + k_3}, \quad (6)$$

where τ_n and τ_p are the SRH pseudo-lifetimes for electrons and holes respectively and k_3 is a constant from the deep trap approximation used by Courtier et al.[3] The intrinsic carrier density n_i is defined by

$$n_i = g_c g_v \exp\left(-\frac{E_G}{2k_B T}\right). \quad (7)$$

Here, g_c and g_v are the density of states in the conduction and valence bands respectively and E_G is the bandgap of the perovskite. Interfacial recombination is determined at the ETL/perovskite and the perovskite/HTL interfaces via

$$R_l(n,p) = \frac{n|_{x=0^-} p|_{x=0^+} - n_i^2}{p|_{x=0^+}/v_{n_E} + n|_{x=0^-}/v_{p_E} + k_1}, \quad (8)$$

where v_{n_E} and v_{p_E} are the electron and hole recombination velocities at the ETL/perovskite interface and $k_1$is a constant from the deep trap approximation at the ETL/perovskite interface. The electron concentration in the ETL at the interface and the hole concentration in the perovskite at the interface are denoted by $n|_{x=0^-}$ and $p|_{x=0^+}$, respectively. Similarly, at the perovskite/HTL interface

$$R_r(n,p) = \frac{n|_{x=b^-} p|_{x=b^+} - n_i^2}{p|_{x=b^+}/v_{n_H} + n|_{x=b^-}/v_{p_H} + k_2}, \quad (9)$$

where v_{n_H} and v_{p_H} are the electron and hole recombination velocities at the perovskite/HTL interface and k_2 is a constant from the deep trap approximation at the

perovskite/HTL interface. The electron concentration in the perovskite at the interface and the hole concentration in the HTL at the interface are denoted by $n|_{x=b^-}$and $p|_{x=b^+}$respectively.

The anion vacancies are limited to the perovskite layer as well as generation and bulk recombination. Hence the conservation equations for electrons in the ETL $(-b_E < x < 0)$ are given by

$$\frac{\partial n}{\partial t} - \frac{1}{q}\frac{\partial j_n}{\partial x} = 0, \qquad j_n = qD_E\left(\frac{\partial n}{\partial x} - \frac{n}{k_B T}\frac{\partial \phi}{\partial x}\right), \tag{9}$$

with

$$\frac{\partial^2 \phi}{\partial x^2} = \frac{q}{\epsilon_E}(n - d_E), \tag{10}$$

where D_E is the electronic diffusion coefficient in the ETL and ϵ_E and d_E are the permittivity and effective doping density of the ETL respectively. Similarly, the conservation equations for holes in the HTL $(b < x < b + b_H)$ are given by

$$\frac{\partial p}{\partial t} + \frac{1}{q}\frac{\partial j_p}{\partial x} = 0, \qquad j_p = -qD_H\left(\frac{\partial p}{\partial x} + \frac{p}{k_B T}\frac{\partial \phi}{\partial x}\right), \tag{11}$$

with

$$\frac{\partial^2 \phi}{\partial x^2} = \frac{q}{\epsilon_H}(d_H - p). \tag{12}$$

Here, D_H denotes the hole diffusion coefficient in the HTL and ϵ_H and d_H are the HTL permittivity and effective doping density respectively. A number of boundary conditions are applied to equations (1-12) to simulate the physics of PSC operation. To model metal contacts at the ETL and HTL edges, we apply

$$\phi|_{x=-b_E} = 0, \quad n|_{x=-b_E} = d_E, \quad \phi|_{x=b+b_H} = V_{ap} - V_{bi}, \quad p|_{x=b+b_H} = d_H. \tag{13}$$

At the ETL/ $MAPbI_3$ interface

$$\phi|_{x=0^-} = \phi|_{x=0^+}, \qquad \epsilon_E \frac{\partial \phi}{\partial x}|_{x=0^-} = \epsilon_p \frac{\partial \phi}{\partial x}|_{x=0^+}, \qquad k_E \mathrm{n}|_{x=0^-} = n|_{x=0^+},$$

$$j_p|_{x=0} = -qR_{I_l}, \qquad F_p|_{x=0} = 0. \tag{14}$$

At the $MAPbI_3$/HTL interface

$$\phi|_{x=b^-} = \phi|_{x=b^+}, \qquad \epsilon_p \frac{\partial \phi}{\partial x}|_{x=b^-} = \epsilon_H \frac{\partial \phi}{\partial x}|_{x=b^+}, \qquad \mathrm{p}|_{x=b^-} = k_H p|_{x=b^+},$$

$$j_n|_{x=b} = -qR_{I_r}, \qquad F_p|_{x=0} = 0. \tag{15}$$

Here, k_E and k_H specify the ratio of the carrier densities at either side of the perovskite and transport layer interface. They are defined by

$$k_E = \frac{g_c}{g_{c,E}} \exp\left(-\frac{E_c - E_{c,E}}{q k_b T}\right), \qquad k_H = \frac{g_v}{g_{v,H}} \exp\left(-\frac{E_v - E_{v,H}}{q k_b T}\right), \tag{16}$$

where g_c and g_v are the density of states of the perovskite conduction and valance bands respectively, $g_{c,E}$ and $g_{v,H}$ are the density of states of the ETL conduction band and HTL valence band respectively, E_c and E_v are the energies of the conduction and valence bands of the perovskite and $E_{c,E}$ and $E_{v,H}$ are the energies of the conduction and valence bands of the ETL and HTL respectively.

For this work, it is assumed that the density of states of the ETL and HTL are equal to the effective doping densities in those layers, i.e. $g_{c,E} = d_E$ and $g_{v,H} = d_H$. As a result, the band edges $E_{c,E}$ and $E_{v,H}$ are equal to the Fermi levels in the ETL and HTL, denoted by E_{fE} and E_{fH}, respectively. Hence, the built-in voltage is given by

$$V_{bi} = \frac{1}{q}(E_{fE} - E_{fH}) = \frac{1}{q}(E_{c,E} - E_{v,H}). \tag{17}$$

An identical model was previously used by Courtier et al.[3]

Equations (1-12) with boundary conditions (13-15) are solved using the open-source numerical solver *IonMonger*.[4]

Derivation of Eqs. (4) and (5) in text

On making the assumption that the electrons and holes are in quasi-equilibrium, the usual assumption when deriving a diode equation, we obtain the relation[5,6]

$$np = N_c N_p exp\left[-\frac{(E_c - E_v) - (E_{F,n} - E_{F,p})}{k_B T}\right] = N_c N_p exp\left[-\frac{E_g - qV}{k_B T}\right] \tag{18}$$

where E_g is the band gap, V is the applied voltage and N_c and N_v are the effective densities of conduction band and valence band states. Since the electrons and holes are not the only charged species, indeed they typically occur at considerably lower densities that the ion vacancies, we cannot appeal to charge neutrality to assert $p \approx n$. However, the density of these two species are usually correlated and so it is not unreasonable to expect that they grow via a power relation $p \approx n^{\alpha\text{-}1}$, for some constant α, such that

$$n = \left(N_c N_p\right)^{1/\alpha} exp\left[-\frac{E_g - qV}{\alpha k_B T}\right] \quad (19)$$

Thus, under these conditions, the recombination current can be related to the applied voltage, using (3) in the main text and (19), via the equation

$$J_{rec} = qdU_{rec} = J_{00} exp\left[-\left(\frac{\gamma}{\alpha}\right)\frac{E_g - qV}{k_B T}\right] \quad (20)$$

The derivative of this equation with respect to voltage gives the recombination resistance:

$$R_{rec} = \left(\frac{\partial J_{rec}}{\partial V}\right)^{-1} = R_{00} exp\left[-\frac{qV}{n_{id} k_B T}\right]; \quad (21)$$

with $n_{id} = \alpha/\gamma$. On imposing open circuit conditions $V = V_{OC}$, for which the total charge generation rate across the cell G is equal to the recombination rate, we find that

$$V_{OC} = \frac{E_g}{q} - \frac{n_{id} k_B T}{q} ln\left(\frac{J_{00}}{qdG}\right) \quad (22)$$

where n_{id}, the so-called ideality factor, is given, as indicated, by $n_{id} = \alpha/\gamma$.

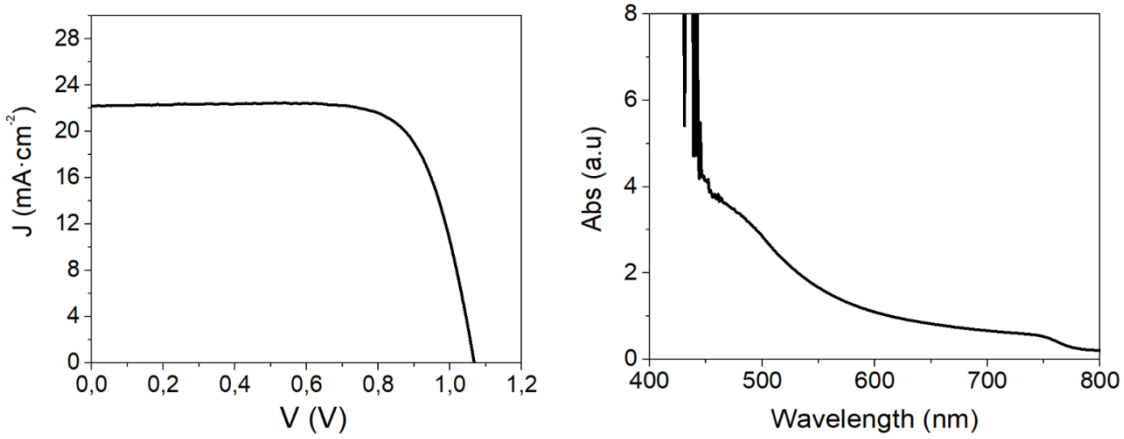

Figure S1. (a) Experimental JV curve at 1 Sun (1000 W/m²) AM1.5G illumination for perovskite solar devices with regular configuration (TiO_2/$MAPbI_3$/Spiro-OMeTAD), **(b)** absorption spectrum of the same device measured at transmittance mode.

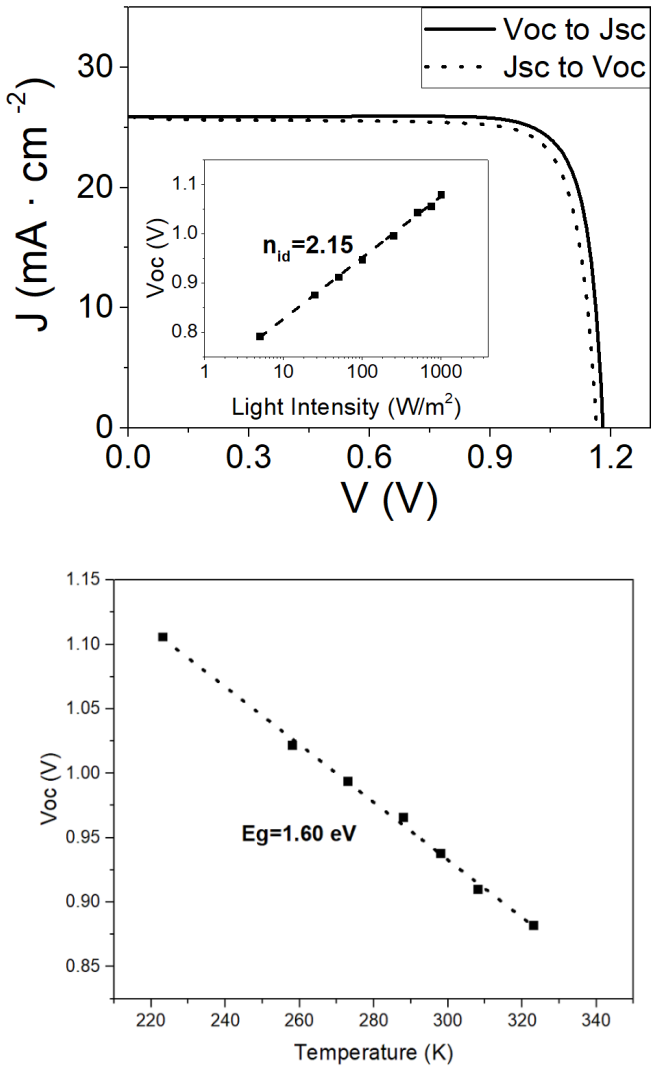

Figure S2. Top: Validation of JV curve as at 1 Sun (1000 W/m^2) AM1.5G illumination for perovskite solar devices with regular configuration as obtained by DD simulation. The inset shows the dependence of the open circuit voltage with respect to illumination and the apparent ideality factor. Bottom: DD numerical prediction of the temperature dependence of the open-circuit photovoltage. Simulations run for the standard parameters of Table 1 in the main paper.

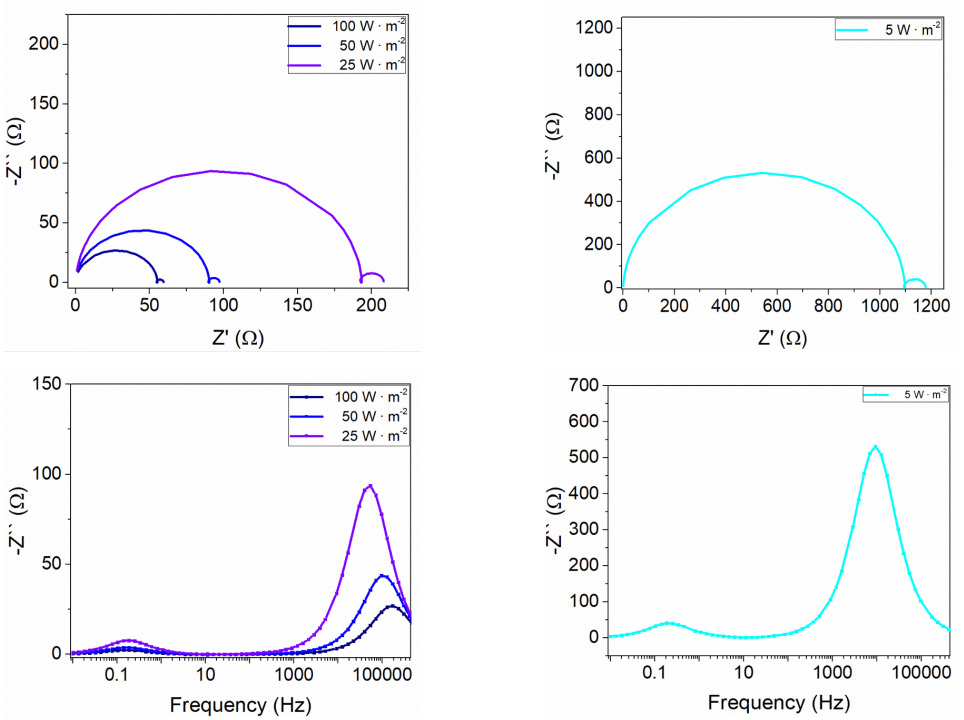

Figure S3. Simulated impedance spectra at open-circuit and variable illumination intensity for perovskite solar devices with regular configuration (TiO2/MAPbI3/Spiro-OMeTAD) using the parameters indicated in Table 1 in the main paper.

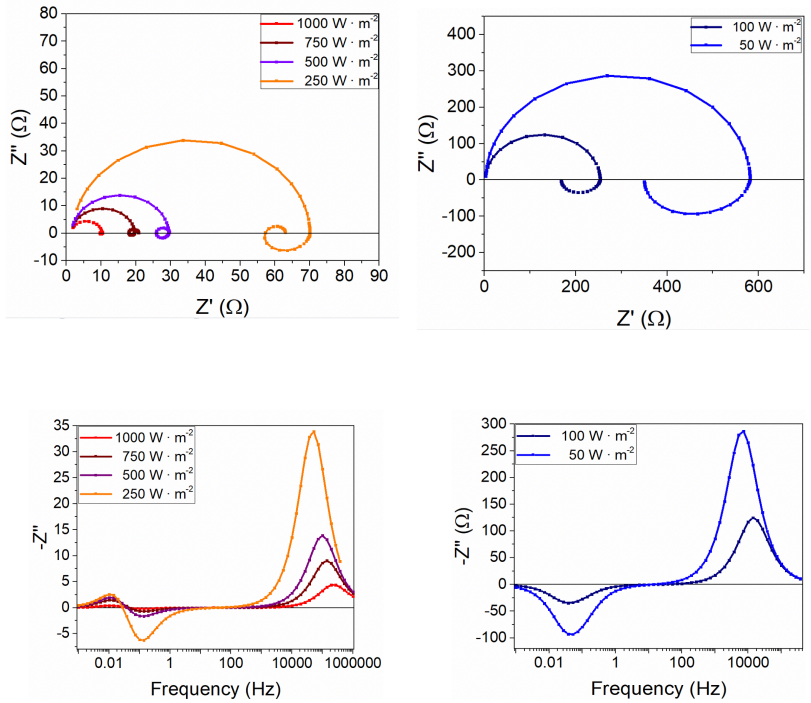

Figure S4. Simulated impedance spectra at open-circuit and variable illumination intensity for perovskite solar devices with inverted configuration (TiO2/MAPbI3/Spiro-OMeTAD). Parameters taken from Ref. 32.

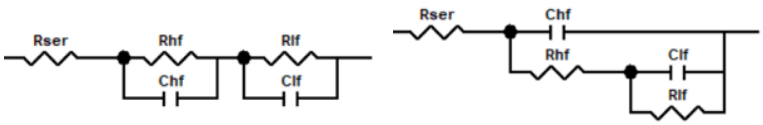

Figure S5. Equivalent circuits used to fit both the experimental and the simulated impedance data.

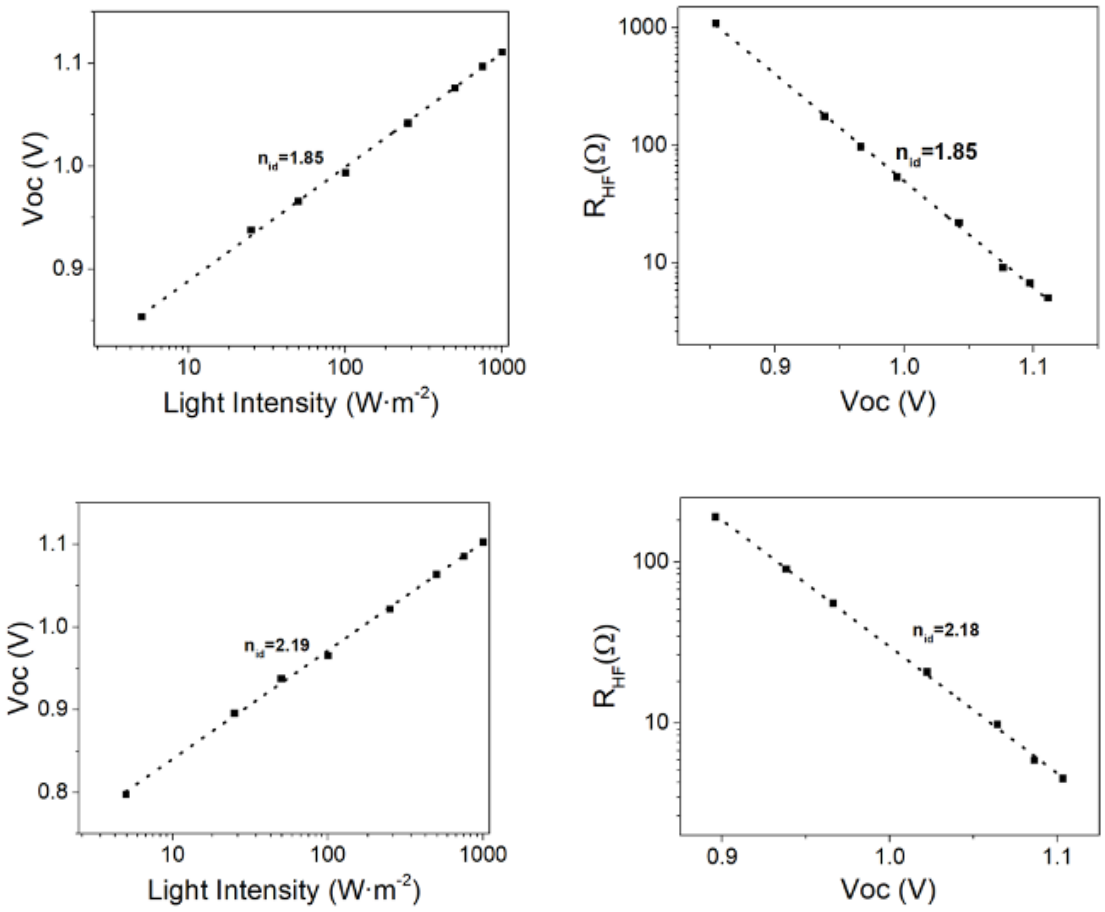

Figure S6. DD numerical prediction of the ideality factor from high frequency resistance and open circuit voltage for two different values of the density of vacancies. **Top**: 10^{25} m^{-3}, **bottom**: 1.8 10^{25} m^{-3}

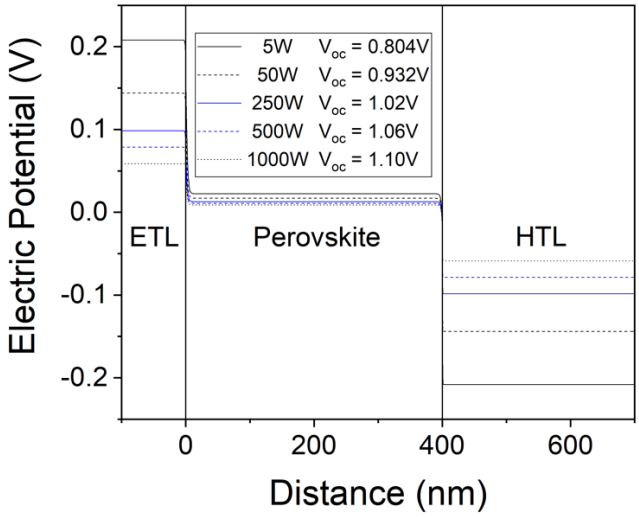

Figure S7. Steady state electric potentials across the cell at different open-circuit voltages with the standard parameter set (Table 1 in the main paper)

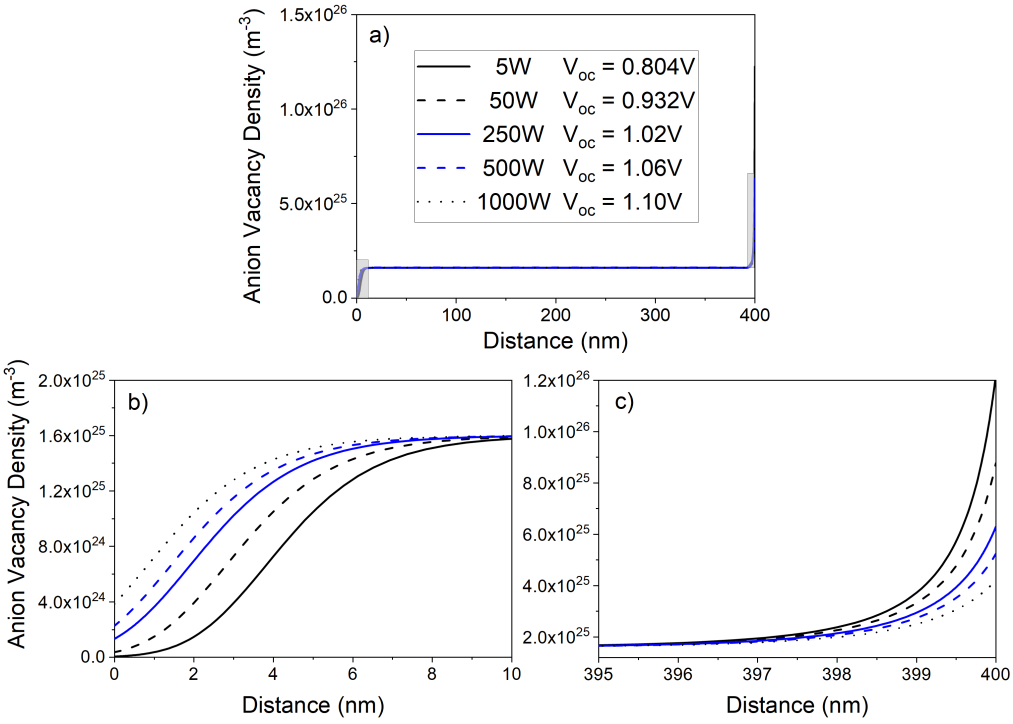

Figure S8. Top: Steady state anion vacancy densities at different open-circuit voltages with the standard parameter set (Table 1 in the main paper). Zoomed images of the shaded Debye layers are shown **below**.

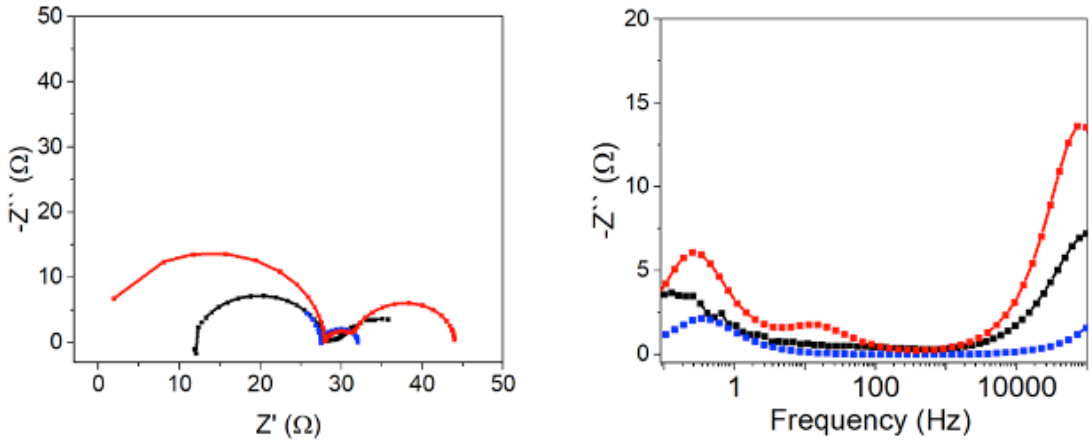

Figure S9. Simulated (red/blue) and experimental (black) impedance spectra at open-circuit for perovskite solar devices with regular configuration (TiO2/MAPbI3/Spiro-OMeTAD) using the parameters indicated in Table 2.

References

1 L. Contreras-Bernal, S. Ramos-Terrón, A. Riquelme, P. P. Boix, J. Idígoras, I. Mora-Seró and J. A. Anta, *J. Mater. Chem. A*, 2019, **7**, 12191–12200.

2 L. Contreras-Bernal, C. Aranda, M. Valles-Pelarda, T. T. Ngo, S. Ramos-Terrón, J. J. Gallardo, J. Navas, A. Guerrero, I. Mora-Seró, J. Idígoras and J. A. Anta, *J. Phys. Chem. C*, , DOI:10.1021/acs.jpcc.8b01558.

3 N. E. Courtier, J. M. Cave, J. M. Foster, A. B. Walker and G. Richardson, *Energy Environ. Sci.*, 2018, **12**, 396–409.

4 N. E. Courtier, J. M. Cave, A. B. Walker, G. Richardson and J. M. Foster, *J. Comput. Electron.*, 2019, **12**, 396–409.

5 L. Contreras-Bernal, M. Salado, A. Todinova, L. Calio, S. Ahmad, J. Idígoras and J. A. Anta, *J. Phys. Chem. C*, 2017, **121**, 9705–9713.

6 J. Nelson, *The Physics of Solar Cells*, Imperial College Press, 1st edn., 2003.